

Inhibition Effect and Mechanism of 2-(3-bromophenyl)-1-phenyl-1H-Benzimidazole on Copper Corrosion in Acidic Solution

Jinliang Zhang^{1,*}, Hao Li²

¹ School of Materials and Chemical Engineering, Ningbo University of Technology, Ningbo Zhejiang 315211, China

² School of Chemistry and Chemical Engineering, Chongqing University, Chongqing, 400044, China

*E-mail: zhangjinliang_nut@126.com (J. Zhang)

Received: 8 January 2020 / Accepted: 14 February 2020 / Published: 10 April 2020

The inhibition effect of (2-(3-Bromophenyl)-1-phenyl-1H-benzimidazole, BPB) was investigated for inhibiting copper corrosion in 0.5 mol L⁻¹ H₂SO₄ solution, compared with traditional corrosion inhibitor benzimidazole (BIM). Various methods were used including electrochemical methods, scanning electron microscope (SEM), Langmuir type adsorption isotherm, quantum chemical calculation, and molecular dynamics simulation. We found that BPB belongs to a mixed type inhibitor. The adsorption of BPB on Cu conforms to a Langmuir adsorption isotherm. The maximum efficiencies of 70.1% for BIM was improved to 97.0% at 5 mmol L⁻¹. SEM confirms the electrochemical results. Molecular chemical calculation further reveals the inhibition mechanism of BPB at microscopic level and explain its greater inhibition ability than BIM.

Keywords: Inhibitor, Pure copper, H₂SO₄, Corrosion, Simulation.

1. INTRODUCTION

Corrosion can affect all metal materials exposed to an aqueous aggressive solution [1-3]. Humankind has to deal with every single day since it could bring serious results. In the chemical cleaning and pickling process, corrosion is always present due to the rapid deterioration of metals contacting acids such as hydrochloric, or sulfuric acid [4-9]. In nowadays, adding corrosion inhibitors has been widely used for slowing down the corrosion of metal in pickling process because of the simple, economical and convenient properties [10-21]. Among many techniques for preventing corrosion of metals, the application of inhibitors is the most efficient method.

As it has great characteristics, and shows high resistance against chemicals, pure copper is an often-used metal in industry. Therefore, copper protection is important. In past decades, various pickling

corrosion inhibitors of pure copper have been continuously studied and applied [22-27]. Many organic compounds have been investigated as effective corrosion inhibitors. These compounds always contain unsaturated bonds and atoms, such as N, S, O and so on, which can accelerate inhibitor molecules to adsorb onto copper surface [28-33], thus expelling the corrosion medium from contacting the metal. Tan et al. studied three 5-phenyltetrazole derivatives towards copper corrosion in H_2SO_4 medium [13]. Electrochemical results show that all these inhibitors adsorbed on Cu surface by Langmuir adsorption to increase the charge transfer resistance. Qiang et al. also prepared carbon quantum dots and ionic liquids as high-efficiency copper corrosion inhibitors in sulfuric acid solution for the first time [34, 35]. He combined experimental and theoretical methods to perform multi-angle calculations at the atomic level and significantly advances the field of organic corrosion inhibitors.

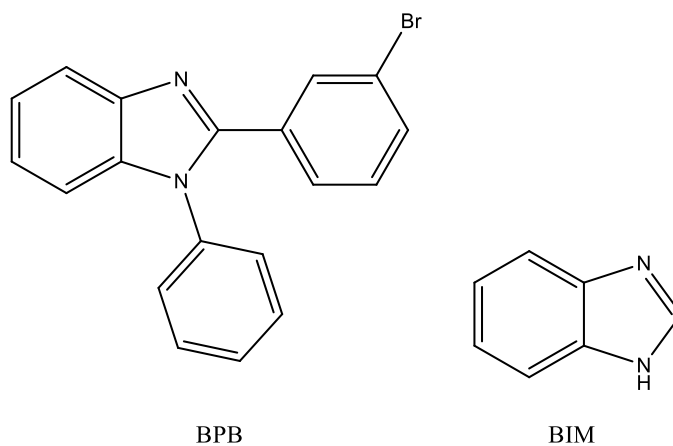


Figure 1. The chemical structures of BPB and BIM.

At this study, we firstly found and investigated benzimidazole (BIM) derivative BPB namely 2-(3-Bromophenyl)-1-phenyl-1H-benzimidazole shown in Fig. 1 as novel efficient inhibitor of copper. Electrochemical impedance measurements (EIS), polarization curves, scanning electron microscope (SEM) were used to compare the inhibition effect of BPB and BIM for copper corrosion in 0.5 mol L^{-1} sulfuric medium. Finally, molecular simulation and DFT calculation were applied to give the explanation of studied inhibitors.

2. EXPERIMENTAL

2.1 Materials

Copper electrode with the purity of more than 99.5% was used. The copper was sealed with epoxy resin with the working surface of $1 \times 1 \text{ cm}$. The copper surface was polished with SiC sandpaper until 2400 mesh. It was degreased with acetone, swashed with deionized water, dried at room temperature. CHI760e electrochemical workstation with a three-electrode system was used, consisting of working electrode (copper), the platinum counter electrode and the reference electrode (saturated calomel electrode). The $0.5 \text{ mol L}^{-1} \text{ H}_2\text{SO}_4$ was prepared using ultrapure water and concentrated H_2SO_4 . BPB was dissolved in $0.5 \text{ mol L}^{-1} \text{ H}_2\text{SO}_4$ ($0.5, 1, 2, \text{ and } 5 \text{ mmol L}^{-1}$).

2.2 Tests

After open circuit potential (OCP) evaluation, AC impedance was tested from 100000 Hz to 0.01 Hz on stable OCP and the excitation signal is 5 mV wave. The polarization curves were measured with a polarization range of ± 250 mV at a scan rate of 1 mV s. The inhibition efficiencies of potentiodynamic polarization are determined as following equation,

$$\eta(\%) = \left(1 - \frac{R_{p,0}}{R_p}\right) \times 100 \quad (1)$$

where R_p and $R_{p,0}$ are the sum of R_f and R_{ct} with and without studied compounds, respectively.

The inhibition efficiency of EIS test can be obtained by following equation:

$$\eta(\%) = \left(1 - \frac{i_{corr}}{i_{corr,0}}\right) \times 100 \quad (2)$$

where $i_{corr,0}$ and i_{corr} is current densities of bare copper and with inhibitor adsorption, respectively.

The surface morphology of copper specimens in the absence and presence of BPB was measured by SEM (JEOL-JSM-7800F). Before testing the SEM, the copper cubes were sanded sequentially to 7000 mesh on sand paper and then immersed in 0.5 mol L⁻¹ sulfuric acid containing and not containing 5 mmol L⁻¹ BPB at 298 K, compared with same concentration of BIM.

2.3 Calculation settings

BPB and BIM molecules were optimized by dmol3 module from MS based on DFT theory. The obtained molecular frontier orbitals were discussed. The DFT parameters including the energy of highest occupied molecular orbital (E_{HOMO}), the energy of lowest unoccupied molecular orbital (E_{LUMO}), energy gap ($\Delta E = E_{LUMO} - E_{HOMO}$), and the dipole moment (μ) were obtained.

The stable adsorption of BPB and BIM molecules on Cu was simulated with Forcite module in MS to observe the interaction between inhibitors and Cu (111) surface. 250 water molecules were added. The calculation parameters were NVT ensemble, 1 fs time step size and 300 ps simulation time. COMPSS force field and Electrostatic and Van der Waals were set. Besides, the maximum number of convergences is 500.

3. RESULTS AND DISCUSSION

3.1 EIS test

EIS is a powerful method to study the corrosion inhibition of pure copper. Fig. 2a shows Nyquist plots for Cu in 0.5 mol L⁻¹ sulfuric acid in the absence and presence of various concentrations of BPB. Fig. 2b shows the comparison of BPB and BIM at concentration of 5 mmol L⁻¹. We can see that the blank spectrum consists a semicircle of capacitive type followed with a Warburg impedance. After the addition of BPB, the Warburg impedance is disappeared and the impedance response was represented by only capacitive type.

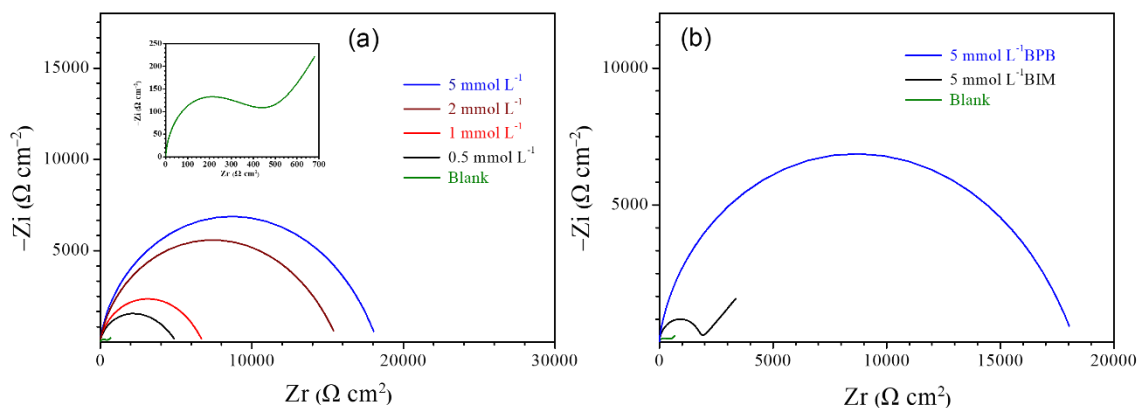


Figure 2. Nyquist diagrams of copper in 0.5 mmol L⁻¹ sulfuric acid (a) with BPB, (b) compared with BIM.

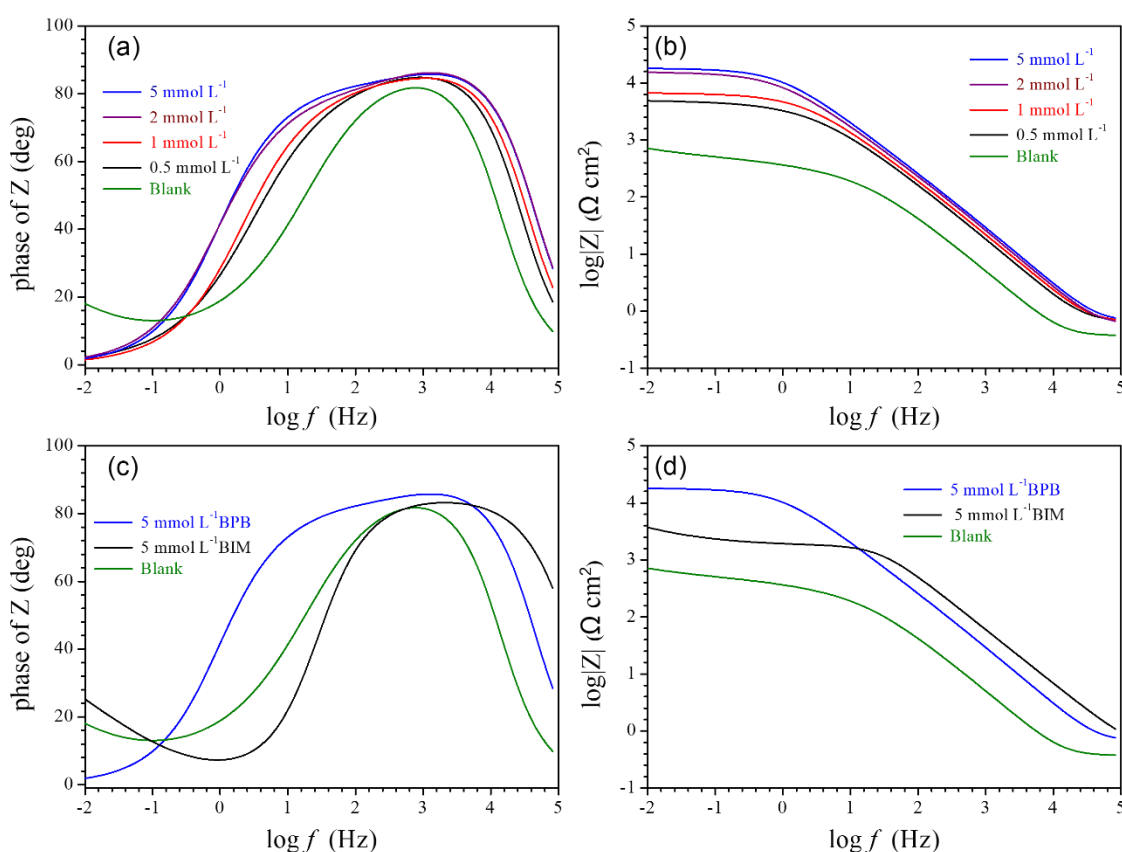


Figure 3. Bode plots of copper in 0.5 mmol L⁻¹ sulfuric acid with (a, b) BPB, (c, d) compared with BIM at 298 K.

However, BIM don't change the spectrum of blank solution due to the loose inhibitor layer. It is well-known that the cathodic reaction of Cu in H₂SO₄ solution at E_{corr} is oxygen reduction being the hydrogen discharge current density negligible as compared to oxygen reduction current density and the anodic reaction is copper dissolution [36]. The presence of the Warburg impedance could be attributed to either the transportation of corrosive ions and soluble corrosion products at the metal/solution interface or the diffusion of dissolved oxygen from the bulk solution to the copper electrode surface.19,20

Besides, increasing BPB concentration lead to the radius of the capacitive arc increases significantly. This is because the BPB adsorption on the surface of copper electrode resulted in the formation of a dense protective inhibitor layer. Thus, the corrosion resistance of the electrode increased and the dissolution of copper became difficult. As shown that with different concentration of BPB inhibitor, the shape of the impedance plot is similar, which present that the corrosion mechanism of Cu was not changed by BPB [37, 38]. We also found that the bigger impedance radius of BPB than BIM at 5 mmol L⁻¹ in Fig. 2b, revealing the greater protection performance of BPB inhibitor than the BIM compound.

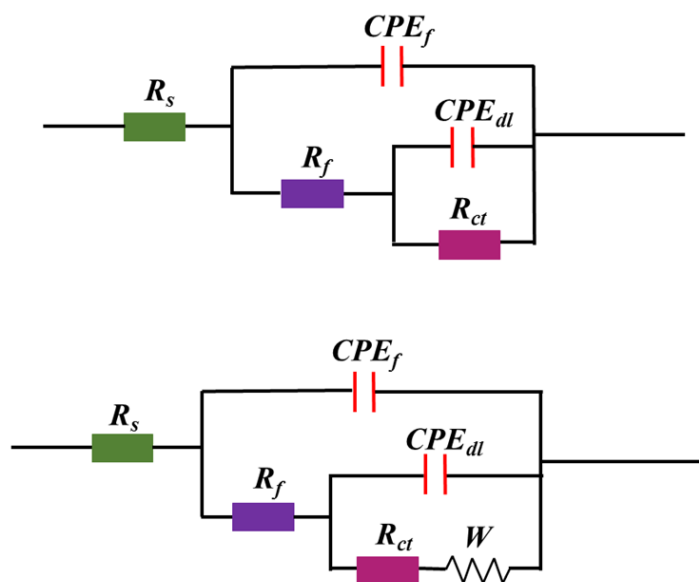


Figure 4. The used equivalent circuit diagrams for AC impedance.

Table 1. EIS parameters for copper in 0.5 mol L⁻¹ sulfuric acid with different BPB concentration compared with 5 mmol L⁻¹ BIM.

	<i>C</i>	<i>R_f</i>	<i>R_{ct}</i>	<i>R_p</i>	<i>C_f</i>	<i>n₁</i>	<i>C_{dl}</i>	<i>n₂</i>	<i>W</i>	<i>η</i> (%)
	(mM)	(Ω cm ²)	(kΩ cm ²)	(kΩ cm ²)	(μF cm ⁻²)		(μF cm ⁻²)			
	Blank	0.4	0.56	0.56	50.1	0.4	62.3	1	1.29	—
BPB	0.5	126	4.91	5.03	8.5	1	44.1	0.54	—	88.9
	1	127	6.66	6.93	7.0	1	23.9	0.62	—	91.9
	2	330	15.3	15.6	6.0	1	16.1	0.67	—	96.4
	5	396	18.0	18.4	5.3	1	11.1	0.65	—	97.0
BIM	5	81	1.79	1.87	14.2	0.95	51.0	0.55	6.47	70.1

Fig. 3 shows Bode plots in the absence and presence of BPB and BIM. The impedance modulus bigger and the phase angle become remarkably larger with increasing concentration of BPB. At the maximum concentration of these compounds, the bigger modulus and phase angle of BPB than BIM can be clearly seen. The equivalent circuits in Fig. 4 were used to simulate the AC impedance data including charge transfer resistance (*R_{ct}*), film resistance (*R_f*) and a constant phase element (*CPE*). Double layer

and film capacitance (C_{dl} and C_f) value were simulated from CPE . The capacitance C was calculated by equation [12, 33]:

$$C = Y_0(\omega)^{n-1} = Y_0(2\pi f_{Zim-Max})^{n-1} \tag{3}$$

After the fitting process, all fitted parameters are obtained and listed in Table 1.

As seen that both values of C_f and C_{dl} decreased dramatically with the concentrations of BPB increases. It can be explained by water molecules on the copper surface replaced by BPB molecules with its addition and increased concentration. Therefore, the protective BPB film can be formed on Cu surface to reduce the copper area exposed to the corrosive medium. Also, the values of R_{ct} and R_f are much larger for inhibited conditions as compared to those values of blank condition. This manifests the formation of BPB-adsorption film on Cu substrate. For BIM, the maximum inhibition efficiency is 70.1% at 5 mmol L⁻¹ BPB. The η value of BPB has been improved remarkably and reaches 97.0% at 5 mmol L⁻¹.

3.2 Potentiodynamic polarization

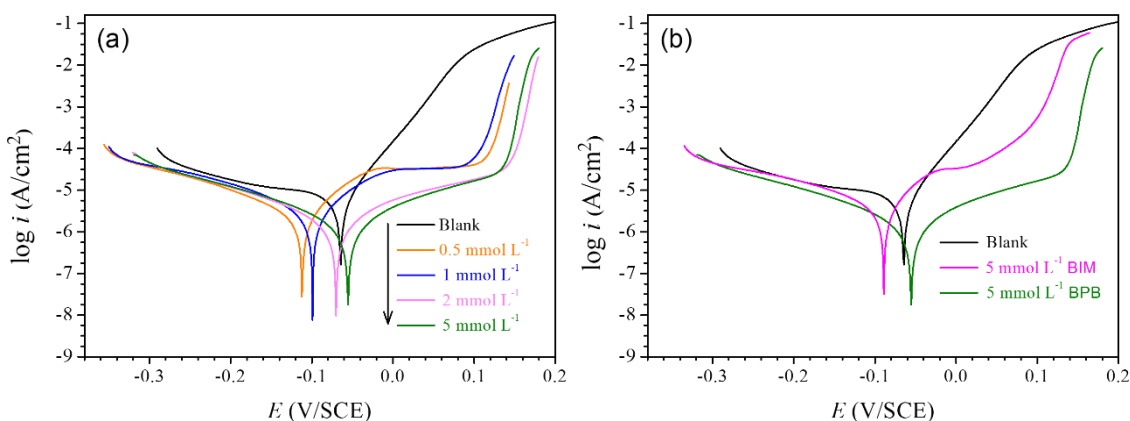


Figure 5. Potentiodynamic polarization curves of copper in 0.5 mmol L⁻¹ sulfuric acid (a) with BPB and the (b) compared with BIM at 298 K.

Fig. 5a shows Tafel plots of copper in 0.5 mol L⁻¹ sulfuric acid with and without BPB at 298 K, Fig. 5b presents the comparison of Tafel plots of BPB and BIM at 5 mmol L⁻¹. The variation of parameters including i_{corr} , η , E_{corr} (corrosion potential), β_a (anodic Tafel slope) and β_c (cathodic Tafel slope) were given in Table 2.

Table 2. Electrochemical parameters of copper in 0.5 mol L⁻¹ sulfuric acid with BPB and BIM at 298 K.

Inhibitor	C(mmol L ⁻¹)	E_{corr} (mV/SCE)	i_{corr} ($\mu A cm^{-2}$)	β_c (mV dec ⁻¹)	β_a (mV dec ⁻¹)	η (%)
	Blank	-64	13.9	-428	41	—
BPB	0.5	-112	3.22	-145	87	76.8
	1	-99	2.78	-114	74	80.0
	2	-70	1.06	-101	98	92.4
	5	-55	0.95	-91	89	93.2
BIM	5	-89	4.51	-142	70	62.1

The corrosion current density decreases significantly with the addition and increasing concentration of BPB from 0.5 mmol L^{-1} to 5 mmol L^{-1} . Anodic and cathodic reaction are reduced and the change of corrosion potential is below than 85 mV, indicating that BPB belongs to a mixed-type corrosion inhibitor [31]. We can see in Fig. 5b, compared with BIM, BPB has better inhibitive performance. In Table 1, i_{corr} values reduce with BPB addition and continue to decrease with incremental concentration of studied BPB. In addition, the η values increase with increasing BPB concentration. At 5 mmol L^{-1} BPB concentration, the traditional corrosion inhibitor BIM only provided best 62.1% protective ability. As a comparison, the inhibition efficiency of BPB can reach the maximum value of 93.2% at 5 mmol L^{-1} . Thus, we can infer that a dense BPB protective film can be formed on Cu to prevent corrosion from acid medium. This is consistent with the EIS results above.

3.3 morphology study

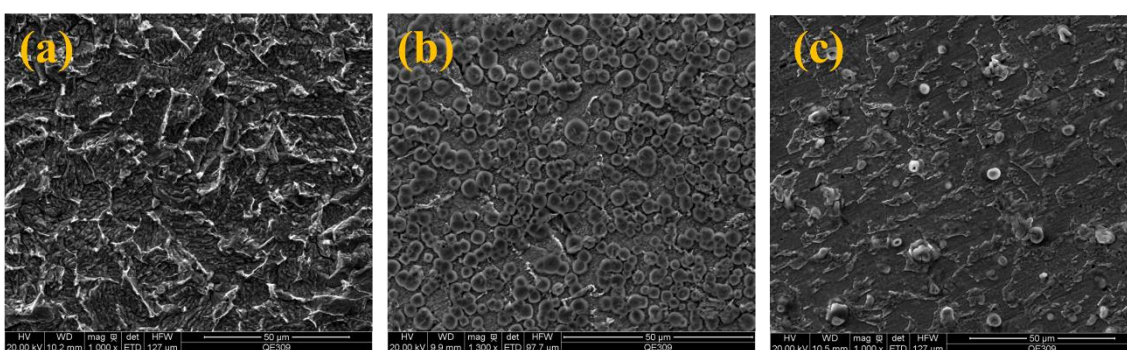


Figure 6. SEM images of copper immersed in (a) $0.5 \text{ mol L}^{-1} \text{ H}_2\text{SO}_4$ and (b) $0.5 \text{ mol L}^{-1} \text{ H}_2\text{SO}_4$ with 5 mmol L^{-1} (b) BIM and (c) BPB respectively for 48 h.

Fig. 6 present SEM images of copper immersed in (a) $0.5 \text{ mol L}^{-1} \text{ H}_2\text{SO}_4$ and (b) $0.5 \text{ mol L}^{-1} \text{ H}_2\text{SO}_4$ with 5 mmol L^{-1} (b) BIM and (c) BPB respectively for 48 h. From Fig. 6a, the copper was corroded and uneven and there were many corrosion pits. After the addition of BIM, the number of corrosion pits on the copper surface was reduced. Besides, it is clear that the entire copper surface becomes most smooth and bright, after the addition of BPB, which indicates that Cu corrosion in $0.5 \text{ mol L}^{-1} \text{ H}_2\text{SO}_4$ solution is effectively inhibited. This shows the greater protection ability of BPB than BIM, which is consistent with electrochemical results.

3.4 Langmuir Adsorption

The adsorption mechanism of organic molecules is displacing the water molecules on metal surface. The adsorption of BPB compound was investigated by several isotherm models. Among numerous of adsorption isotherms, Langmuir model showed the best fit (Fig. 7) of data from potentiodynamic polarization tests. Besides, the Langmuir is expressed by the formula (4) [39, 40]:

$$C/\theta = 1/K_{ads} + C \quad (4)$$

where K_{ads} is equilibrium constant of adsorption, abscissa is C and ordinate is C/θ , intercept is shown as $1/K_{ads}$.

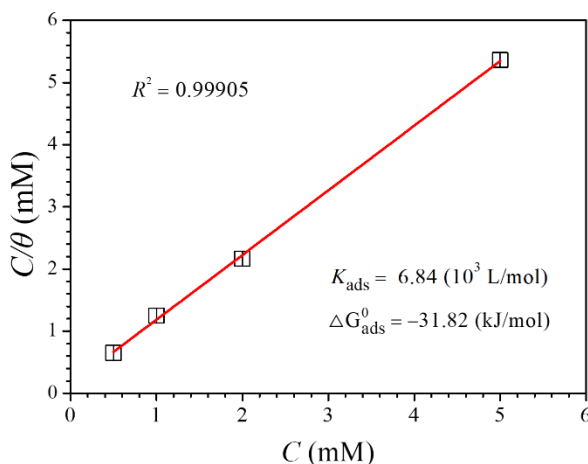


Figure 7. Langmuir adsorption isotherm of copper with addition of BPB in 0.5 mmol L⁻¹ sulfuric acid at 298 K.

As observed in Fig. 7, the regression coefficient (R^2) is close to 1, which indicates that the adsorption of BPB obeys Langmuir isotherm. The expression of standard adsorption Gibbs free energy (ΔG_{ads}^0) is formula (5) [41]:

$$K_{ads} = 1/55.5 \exp(-\Delta G_{ads}^0 / RT) \tag{5}$$

Comparing with previous work, if the ΔG_{ads}^0 of the studied inhibitors are more negative, the adsorption of these compounds on copper surface is more spontaneous [2]. We found that in Fig. 7, the calculated ΔG_{ads}^0 values for BPB is $-31.82 \text{ kJ mol}^{-1}$, indicating the spontaneous adsorption process of BPB molecules. It is noted that ΔG_{ads}^0 values less negative than -20 kJ mol^{-1} indicates the process involved physical adsorption. If the ΔG_{ads}^0 values are more negative than -40 kJ mol^{-1} , the chemisorption can be inferred. We can clearly see the ΔG_{ads}^0 value is between -20 and -40 kJ mol^{-1} in Fig. 7, which indicates the mixed adsorption type of BPB molecules on Cu

3.5 Quantum Chemical Calculation

The frontier molecular orbitals (FMO) of metallic surface and inhibitor molecules undergo donor–acceptor interaction. Thus, DFT calculation was used to obtain the adsorption and inhibition mechanism of BPB on copper corrosion. The FMO graph are shown in Fig. 8 and DFT parameters are listed in Table 3.

Table 3. The DFT parameters of BPB and BIM.

Inhibitor	$E_{HOMO}(eV)$	$E_{LUMO}(eV)$	$\Delta E(eV)$	$\mu(D)$
BPB	-5.60	-2.27	3.33	7.16
BIM	-5.58	-1.42	4.16	5.04

In Fig. 8, HOMO and LOMO orbitals of BPB are distributed on larger area than those of BIM, indicating the stronger interaction with Cu substrate. Based on FMO theory, higher energy of E_{HOMO}

values indicate a stronger electron-donating ability, and lower E_{LUMO} energy is related to a stronger electron-accepting ability [42].

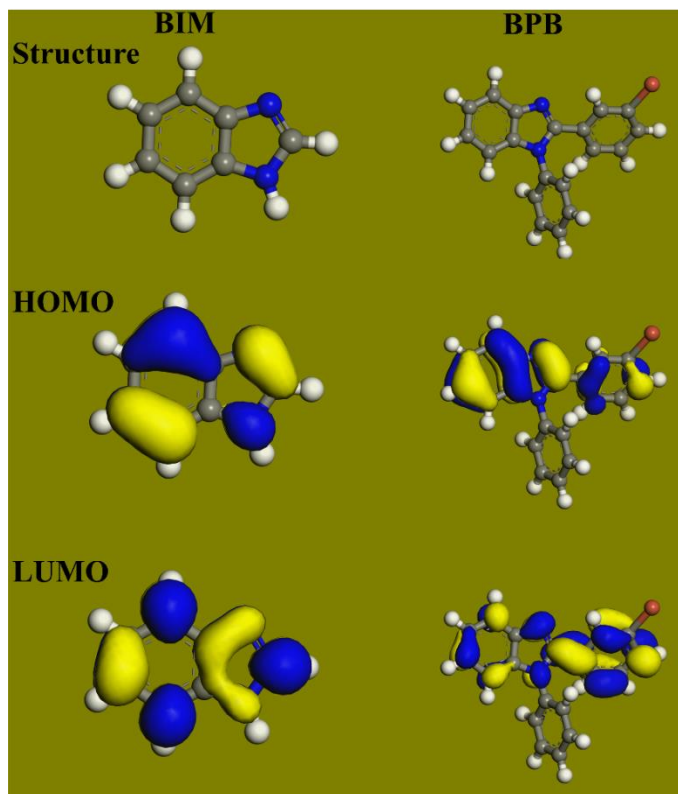


Figure 8. The molecular structure and frontier orbital diagrams of BIM and BPB respectively.

Therefore, it is generally believed that the smaller energy gap value represents stronger interaction with metal and thus have better corrosion inhibition performance. In present study, the lower ΔE value of 3.33 eV for BPB can be seen than 4.16 eV for BIM in Table 3. This presents greater inhibitive performance of BPB than BIM for copper corrosion. In addition, the μ values of two compounds are 7.16 D (BPB), 5.04 D (BIM) respectively. It is noted that the higher dipole moment value indicates higher corrosion inhibition capability, which explain the great inhibitive ability of BPB for copper corrosion than BIM.

3.6 Molecular dynamics simulation

Molecular dynamics simulation was as a powerful simulation tool to study the adsorption behavior of inhibitor molecules on metal surface. The stable adsorption configurations of BPB and BIM adsorbed on Cu (111) are shown in Fig. 9. We can see that two molecules are both adsorbed parallelly on Cu. This mode can minimize the attack of corrosion particles to metal surface thus give highest protective ability. Besides, the binding energy (E_{binding}) values between Cu and inhibitor molecules were also calculated by the formula in the literature. The obtained values of E_{binding} is 53.8 kJ/mol for BIM and 85.7 kcal/mol for BPB respectively. Therefore, BPB can adsorb onto the copper surface easily than

BIM and thus BPB inhibitor can exhibit superior inhibition performance than BIM. The theoretical results can confirm the experimental inhibition performance rank.

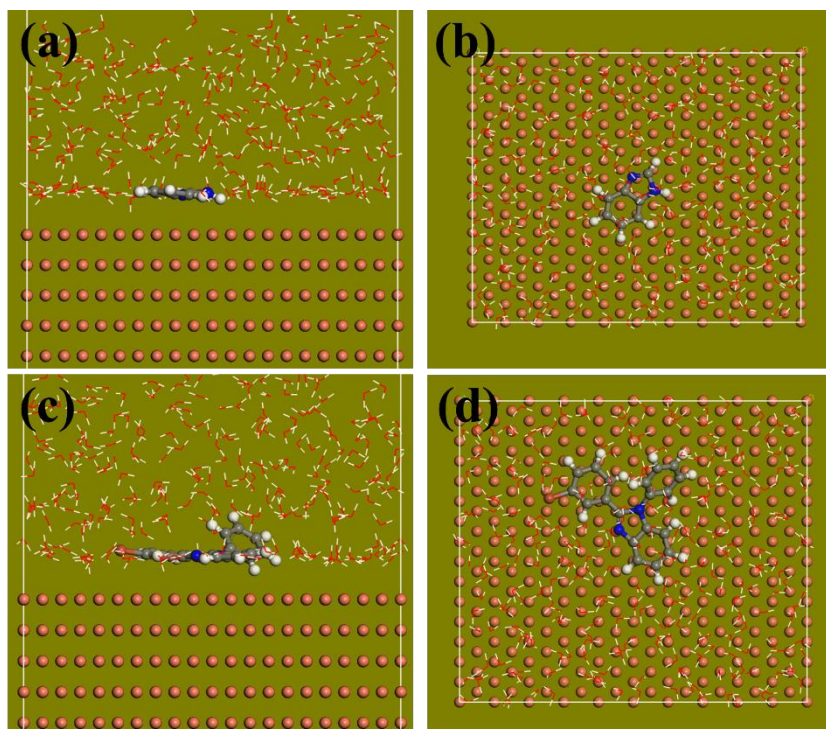


Figure 9. The stable adsorbed configurations of BIM and BPB molecules on Cu (111) considering water effect, respectively.

4. CONCLUSIONS

The results obtained from potentiodynamic polarization and EIS support the greater protective ability of BPB than BIM for copper in $0.5 \text{ mol L}^{-1} \text{ H}_2\text{SO}_4$ solution. Polarization results indicate that BPB is a mixed type inhibitor suppressing both cathodic and anodic reactions. From EIS results, with presence of 5 mmol L^{-1} BPB, the maximum efficiency of 97.0% was obtained, whereas 5 mmol L^{-1} BIM only have 70.1%. Besides, BPB also obeys Langmuir adsorption isotherm and the adsorption of BPB on metal surface is spontaneous. SEM graphs show that copper surface is protected by BPB. Quantum chemical study reveals smaller energy gap of BPB than BIM, which agree well with electrochemical results. Molecular dynamics simulation also supports the experimental data above.

References

1. I.B. Onyeachu, I.B. Obot, A.A. Sorour, M.I. Abdul-Rashid, *Corros. Sci.*, 150 (2019) 183-193.
2. Y.J. Qiang, S.T. Zhang, S.Y. Xu, L.L. Yin, *RSC Adv.*, 5 (2015) 63866-63873.
3. Y. Qiang, S. Zhang, S. Xu, L. Guo, N. Chen, I.B. Obot, *Inter. J. Electrochem. Sci.*, 11 (2016) 3147-3163.
4. B. Tan, S. Zhang, Y. Qiang, W. Li, H. Li, L. Feng, L. Guo, C. Xu, S. Chen, G. Zhang, *J. Mol. Liq.*, 298 (2020).
5. J. Zhang, *Inter. J. Electrochem. Sci.*, 13 (2018) 8645-8656.
6. E. A. Flores-Frias, *Inter. J. Electrochem. Sci.*, 14 (2019) 5026-5041.

7. Z. Xiao, *Inter. J. Electrochem. Sci.*, 14 (2019) 4705-4717.
8. S. Xu, *Inter. J. Electrochem. Sci.*, 14 (2019) 5777-5793.
9. S. Y. Al-Nami, *Inter. J. Electrochem. Sci.*, 14 (2019) 3986-4002.
10. C. Verma, I.B. Obot, I. Bahadur, E.-S.M. Sherif, E.E. Ebenso, *Appl. Surf. Sci.*, 457 (2018) 134-149.
11. Y. Qiang, L. Guo, S. Zhang, W. Li, S. Yu, J. Tan, *Sci. Rep.*, 6 (2016) 33305.
12. Y. Qiang, S. Zhang, B. Tan, S. Chen, *Corros. Sci.*, 133 (2018) 6-16.
13. B. Tan, S. Zhang, H. Liu, Y. Qiang, W. Li, L. Guo, S. Chen, *J. Taiwan Instit. Chem. Eng.*, 102 (2019) 424-437.
14. L. Feng, S. Zhang, Y. Qiang, S. Xu, B. Tan, S. Chen, *Mater. Chem. Phys.*, 215 (2018) 229-241.
15. M.A. Amin, K.F. Khaled, *Corros. Sci.*, 52 (2010) 1194-1204.
16. K.F. Khaled, *Corros. Sci.*, 52 (2010) 3225-3234.
17. H. Otmacic Curkovic, E. Stupnisek-Lisac, H. Takenouti, *Corros. Sci.*, 52 (2010) 398-405.
18. S. Yuan, S.O. Pehkonen, B. Liang, Y.P. Ting, K.G. Neoh, E.T. Kang, *Corros. Sci.*, 52 (2010) 1958-1968.
19. N. V. Likhanova, *Inter. J. Electrochem. Sci.*, 14 (2019) 2655-2671.
20. C. Wang, *Inter. J. Electrochem. Sci.*, 14 (2019) 3443-3454.
21. X. Wang, *Inter. J. Electrochem. Sci.*, 14 (2019) 1178-1196.
22. Sudheer, M.A. Quraishi, *Corros. Sci.*, 70 (2013) 161-169.
23. M. Mousavi, T. Baghcoli, *Corros. Sci.*, 105 (2016) 170-176.
24. Y. Qiang, S. Zhang, L. Wang, *Appl. Surf. Sci.*, 492 (2019) 228-238.
25. Y. Qiang, S. Zhang, Q. Xiang, B. Tan, W. Li, S. Chen, L. Guo, *RSC Adv.*, 8 (2018) 38860-38871.
26. K.F. Khaled, N. Hackerman, *Electrochim. Acta.*, 49 (2004) 485-495.
27. L. Larabi, O. Benali, S.M. Mekelleche, Y. Harek, *Appl. Surf. Sci.*, 253 (2006) 1371-1378.
28. Y. Qiang, S. Zhang, S. Xu, W. Li, *J. Colloid Interf. Sci.*, 472 (2016) 52-59.
29. Y. Qiang, S. Zhang, L. Guo, S. Xu, L. Feng, I.B. Obot, S. Chen, *J. Clean Prod.*, 152 (2017) 17-25.
30. B. Tan, S. Zhang, Y. Qiang, L. Feng, C. Liao, Y. Xu, S. Chen, *J. Mol. Liq.*, 248 (2017) 902-910.
31. Y. Qiang, S. Zhang, S. Yan, X. Zou, S. Chen, *Corros. Sci.*, 126 (2017) 295-304.
32. B. Tan, S. Zhang, Y. Qiang, W. Li, H. Liu, C. Xu, S. Chen, *J. Mol. Liq.*, 286 (2019).
33. Y. Qiang, S. Fu, S. Zhang, S. Chen, X. Zou, *Corros. Sci.*, 140 (2018) 111-121.
34. Y. Qiang, S. Zhang, L. Guo, X. Zheng, B. Xiang, S. Chen, *Corros. Sci.*, 119 (2017) 68-78.
35. Y. Qiang, S. Zhang, H. Zhao, B. Tan, L. Wang, *Corros. Sci.*, 161 (2019).
36. Z. Tao, W. He, S. Wang, G. Zhou, *Ind. Eng. Chem. Res.*, 52 (2013) 17891-17899.
37. M.B.P. Mihajlovic, M.B. Radovanovic, Z.Z. Tasic, M.M. Antonijevic, *J. Mol. Liq.*, 225 (2017) 127-136.
38. J. Wang, Y. Qiang, L. Jiang, B. Xiang, S. Chen, S. Xing, Y. Wang, Y. Wang, *J. Mol. Liq.*, 271 (2018) 959-969.
39. A. Singh, K.R. Ansari, M.A. Quraishi, H. Lgaz, Y. Lin, *J. Alloy Compd.*, 762 (2018) 347-362.
40. Z. Mohammadi, M. Rahsepar, *J. Alloy Compd.*, 770 (2019) 669-678.
41. R. Kumar, O.S. Yadav, G. Singh, *J. Mol. Liq.*, 237 (2017) 413-427.
42. P. Dohare, K.R. Ansari, M.A. Quraishi, I.B. Obot, *J. Ind. Eng. Chem.*, 52 (2017) 197-210